Applied Catalysis B: Environmental 259 (2019) 118026

Contents lists available at ScienceDirect

Applied Catalysis B: Environmental

journal homepage: www.elsevier.com/locate/apcatb

Unravelling the effects of layered supports on Ru nanoparticles for enhancing N_2 reduction in photocatalytic ammonia synthesis

Huimin Liu[a,b,1], Ping Wu[b,1], Haitao Li[a], Zibin Chen[c], Lizhuo Wang[a], Xin Zeng[a], Yuxiang Zhu[d], Yijiao Jiang[d], Xiaozhou Liao[c], Brian S. Haynes[a], Jinhua Ye[e,*], Catherine Stampfl[b,*], Jun Huang[a,*]

[a] Laboratory for Catalysis Engineering, School of Chemical and Biomolecular Engineering, Sydney Nano Institute, The University of Sydney, Chemical Engineering Building J01, Sydney, New South Wales 2006, Australia
[b] School of Physics, Sydney Nano Institute, The University of Sydney, Sydney, New South Wales, 2006, Australia
[c] School of Aerospace, Mechanical and Mechatronic Engineering, Sydney Nano Institute, The University of Sydney, Sydney, New South Wales, 2006, Australia
[d] Department of Engineering, Macquarie University, Sydney, New South Wales, 2109, Australia
[e] International Center for Materials Nanoarchitectonics (WPI-MANA), National Institute for Materials Science (NIMS), 1-1 Namiki, Tsukuba, Ibaraki, 305-0044, Japan

ARTICLE INFO

Keywords:
Ammonia synthesis
Layered support
Ru-based catalysts
Synergy effects between metal and support
N_2 activation

ABSTRACT

Harnessing the vast supply of solar energy as the driving force to produce ammonia from abundant nitrogen gas and water is beneficial for both relieving energy demands and developing sustainable chemical industry. Bulk carbon nitride (B-g-C_3N_4), exfoliated carbon nitride (E-g-C_3N_4) and graphite (g-C) supported Ru-K catalysts, denoted as Ru-K/B-g-C_3N_4, Ru-K/E-g-C_3N_4 and Ru-K/g-C, respectively, with the layered materials serving both as supports and light harvesters, were designed for photocatalytic ammonia synthesis. It was discovered that, besides the light harvesting properties of the catalysts which played roles in photocatalytic reactions, the structure of the supports influenced greatly the preferential locations of Ru species, which further exerted effects on the N_2 activation process and ultimately impacted the ammonia production rate. The fine Ru nanoparticles uniformly and randomly dispersed on the monolayered E-g-C_3N_4 did not provide outstanding activity in ammonia photosynthesis; in contrast, Ru nanoparticles at the step edges of bulk g-C_3N_4 exhibited lower overall barriers for N_2 activation and a much enhanced photocatalytic ammonia synthesis rate due to the synergy effects between metal and support as confirmed by density functional theory (DFT) calculations. The discovery of the relationship between reactivity and support geometry in this study will be important in guiding the rational predesign of efficient photocatalysts.

1. Introduction

Owing to its use in the fertilizer industry and in creating building blocks for the synthesis of various pharmaceutical products, ammonia (NH_3) is recognized as one of the mainstays in the modern world, with 160 million tons of ammonia being synthesized per year [1–4]. However, the industrialized Haber-Bosch process suffers from a number of disadvantages, such as using high value-added clean energy H_2 and requiring harsh reaction conditions (temperatures: 400–500 °C and pressures: > 60 bar) [5,6]. In this respect, it will be of great significance to develop a low-cost approach for ammonia synthesis, which could be carried out under mild reaction conditions.

Photocatalytical reduction of nitrogen with water is a promising alternative route for ammonia synthesis. On one hand, water, the cheapest and most abundant hydrogenated resource, has proven to be a favourable substitute for H_2 in ammonia synthesis in several pioneering studies [7,8]; and on the other hand, photoreduction of nitrogen to ammonia using solar light is a sustainable and green ammonia synthesis route [9–11]. Several semiconductors, including bismuth oxyhalides, titanium dioxide and ultrafine Bi_5O_7Br, have been used for photocatalytic ammonia production [7,10,11]. Nevertheless, the efficiencies of these photocatalysts are still low. Therefore, it remains of great importance to develop a photocatalyst which could drive the nitrogen reduction process efficiently.

For the photocatalytic ammonia synthesis process, the cleavage of strongly bonded N ≡ N bond (945 kJ mol^{-1}) is the rate determining step [12–14]. Previous research has revealed that high photocatalytic nitrogen reduction activities and ammonia synthesis capacities could be

* Corresponding authors.
E-mail addresses: Jinhua.Ye@nims.go.jp (J. Ye), Catherine.stampfl@sydney.edu.au (C. Stampfl), Jun.huang@sydney.edu.au (J. Huang).
[1] These authors contributed equally to this work. The manuscript was written through contributions of all authors.

https://doi.org/10.1016/j.apcatb.2019.118026
Received 27 March 2019; Received in revised form 21 July 2019; Accepted 27 July 2019
Available online 02 August 2019
0926-3373/

achieved by introducing transition metals, such as Fe or Ru, to semiconductors for promoting the N≡N cleavage process [15–21]. In comparison to Fe, Ru is more favourable for N≡N activation because it requires relatively mild reaction conditions [15,16] and high catalytic activities can be achieved by adding alkali or alkaline earth metals, such as K or Ba, as promoters.

It has been widely reported that the architecture and interaction between supports and metal nanoparticles could significantly influence the activities of metal nanoparticles in the catalytic reactions [22–25]. For photocatalytic ammonia synthesis via N_2 fixation, although several studies have been carried out over Ru/semiconductor catalysts [26–29], to the best of our knowledge, there have been no reports on investigating the structural effects of the semiconductor support on the photocatalytic performance. Therefore, it is important to investigate this unexplored area, since its success will definitely contribute new knowledge and foster the development of the targeted research area.

Two dimensional semiconductors have been widely used as supports of photocatalysts in the form of either their bulk particles or exfoliated monolayers, with monolayered supports generally being considered to contribute higher activities than their bulk counterparts [30–32]. Among the numerous two dimensional semiconductors, graphitic carbon nitride ($g\text{-}C_3N_4$) is attracting significant attention and has been extensively investigated in the area of photocatalysis because of its remarkable light harvesting capacity in the visible light region [33–35]. Further, $g\text{-}C_3N_4$, including both bulk $g\text{-}C_3N_4$ ($B\text{-}g\text{-}C_3N_4$) and exfoliated $g\text{-}C_3N_4$ ($E\text{-}g\text{-}C_3N_4$), has proven to be capable of activating nitrogen with light irradiation [36–39]. In the present study, both bulk and exfoliated forms were adopted as supports for Ru-based catalysts for photocatalytic ammonia production. In addition, commercial graphite (g-C), a material with a layered structure similar to that of $B\text{-}g\text{-}C_3N_4$ but with a very different response to light irradiation, was employed as a reference support. The physicochemical and photoelectrical properties of the supports and catalysts were characterized in detail to establish the relationship between reactivity and support/catalyst geometry with the assistance of theoretical simulations, which will be important in guiding the rational predesign of efficient photocatalysts for ammonia synthesis.

2. Experiment

2.1. Catalyst preparation

Urea, iso-propanol, KNO_3, $RuCl_3$ and g-C were commercial from Sigma-Aldrich and used as received. Bulk carbon nitride ($B\text{-}g\text{-}C_3N_4$) was prepared by thermally decomposing urea at 550 °C for 4 h [40]. $E\text{-}g\text{-}C_3N_4$ was synthesized by exfoliating $B\text{-}g\text{-}C_3N_4$ by the ultrasonic method [41]. Typically, 100 mg $B\text{-}g\text{-}C_3N_4$ was dispersed in 100 ml iso-propanol, and sonicated for 10 h. The suspension was subsequently centrifuged at 5000 rpm and 22000 rpm, respectively, to remove the un-exfoliated $B\text{-}g\text{-}C_3N_4$. The precipitate was then dried at 80 °C to obtain $E\text{-}g\text{-}C_3N_4$.

Catalysts $Ru\text{-}K/B\text{-}g\text{-}C_3N_4$, $Ru\text{-}K/E\text{-}g\text{-}C_3N_4$ and Ru-K/g-C were prepared via incipient wetness impregnation method in consecutive steps, firstly with KNO_3 followed by $RuCl_3$ solution. In the study, the theoretical loadings of K and Ru were controlled as 5.0 wt% and 2.0 wt%, respectively. Before characterization and reaction evaluation, the catalysts were calcined in 5% H_2/Ar at 400 °C for 4 h to remove Cl residue and reduce Ru to the metallic state.

2.2. Catalyst characterization

The crystalline structures of the catalysts were analysed by an X-ray diffractometer (XRD, SIEMENS D5000) using Cu Kα radiation (wavelength of 0.1542 nm). The surface area, average pore size, and total pore volume of the samples were determined by measuring the N_2 adsorption-desorption isotherms on an Autosorb IQ-C system. The light absorption properties of the catalysts were carried out over a UV–vis spectroscopy (Shimadzu, UV-3800 Plus). The morphology of the supports and catalysts were characterized by transmission electron microscopy (TEM, JEOL 3000). The actual contents of Ru and K over the catalysts, as well as the leaching of Ru and K over the catalysts during reaction evaluation, were analysed by inductively coupled plasma atomic emission spectroscopy (ICP-AES, Varian 720-ES). The photocurrents of the supports and catalysts were measured on a CHI electrochemical analyser using a standard three-electrode mode with 0.5 M Na_2SO_4 solution as the electrolyte.

2.3. Catalyst evaluation

The catalytic performance for the ammonia synthesis reaction was carried out in a 100 ml Teflon-lined, quartz-windowed autoclave. 3.0 mg of the catalyst was dispersed into 15.0 ml deionized water, with 1.0 ml methanol serving as the sacrificial agent. The autoclave was exchanged by 2.0 bar N_2 ten times to remove inside residual air and then refilled by 2.0 bar N_2. The reaction was maintained for several hours with stiring and light irradiation (PE300 Xe lamp). The amount of ammonia production was identified by the indophenol blue method. As reference, the catalytic performance of $Ru\text{-}K/B\text{-}g\text{-}C_3N_4$ and $Ru\text{-}K/E\text{-}g\text{-}C_3N_4$ for the hydrogen evolution reaction were also carried out, with the procedure the same as the one for the ammonia synthesis process, except that Ar, instead of N_2, was used.

2.4. Theoretical calculations

Spin-polarized density functional theory (DFT) calculations were performed using the VASP software. [42,43] The generalized gradient approximation of Perdew, Burke and Ernzerhof (PBE) [44] was used for the exchange-correlation functional. The kinetic energy cut-offs were well tested to yield good convergence of the total energy, where 500 eV was used for all calculations. To correctly describe the strong van der Waals interactions between the neighboring $g\text{-}C_3N_4$ layers, the DFT-D_3 approach of Grimme was applied. [45] A Monkhorst-Pack grid was used and the mesh of k-points ($3 \times 3 \times 1$ for $E\text{-}g\text{-}C_3N_4$ and $1 \times 3 \times 1$ for $B\text{-}g\text{-}C_3N_4$) was well tested for the structure relaxation and the total energy calculations. The climbing image nudged elastic band (CINEB) method was used for transition-state searches and barrier height determination. [46] Residual forces were within 0.02 eV/Å for geometry optimizations and 0.03 eV/Å for transition-state location.

The calculated lattice constants of bulk $g\text{-}C_3N_4$ are a = b = 7.13Å and c = 3.245 Å, in good agreement with the previous theoretical calculations (a = b = 7.178 Å, c = 3.297 Å [47] and a = b = 7.11 Å, c = 3.19 Å [48]). The adsorption energy was defined as $E_{abs} = E_{total} - E_{species} - E_{sub}$, where E_{total}, E_{sub} and $E_{species}$ are the total energy of the whole system, the clean support surface, and reaction gas or metal cluster in vacuum, respectively.

2.5. Calculation of the size of $[Ru(H_2O)_6]^{3+}$

The precursors in solution exist as $[Ru(H_2O)_6]^{3+}$. $[Ru(H_2O)_6]^{3+}$ is octahedral, with a Ru-O bond length of 0.214 nm [49], so the diameter size of $[Ru(H_2O)_6]^{3+}$ would be at least 0.42 nm (0.428nm = 2 × 0.214 nm).

3. Results and discussion

The XRD pattern of commercial g-C revealed the representative diffraction peak for carbon based materials at 27.3° (Fig. 1a) [50]. As-prepared $B\text{-}g\text{-}C_3N_4$ and $E\text{-}g\text{-}C_3N_4$ exhibited the typical diffraction feature of $g\text{-}C_3N_4$ at 13.9° and 27.8° (Fig. 1a), with the two peaks resulting from the graphite structure and tri-s-triazine units, respectively [33–39]. The successful exfoliation of $E\text{-}g\text{-}C_3N_4$ was confirmed by comparing its properties with its precursor $B\text{-}g\text{-}C_3N_4$. As shown in Table 1 and Fig. S1, the surface area is increased from 35.3 to

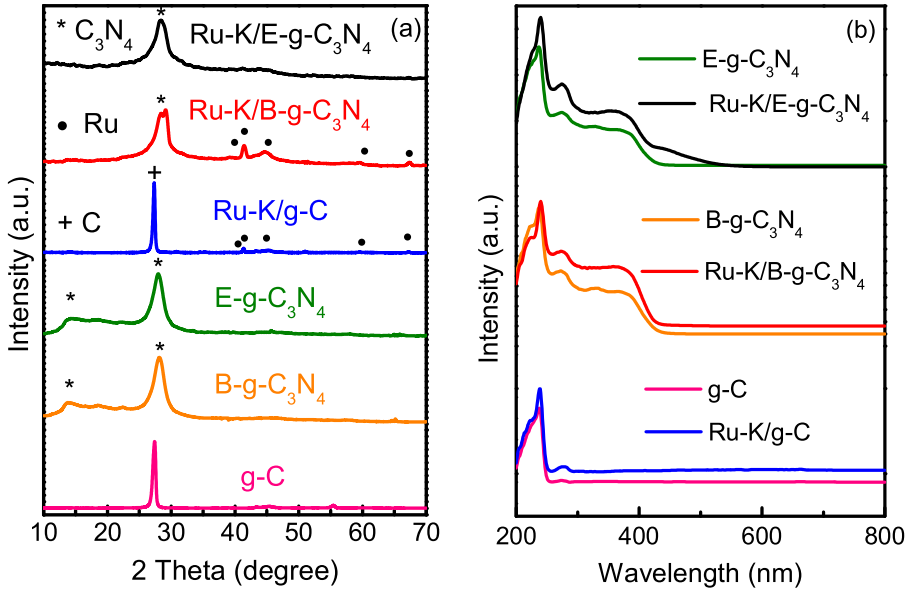

Fig. 1. (a) XRD diffraction patterns (the symbols *, · and + represent C_3N_4, Ru and C, respectively), and (b) UV–vis spectra of supports and catalysts.

Table 1
Physicochemical properties of the supports and catalysts.

Support/Catalyst	S_{BET} ($m^2\,g^{-1}$)[a]	Ru content (wt. %)[b]	K content (wt. %)[b]
graphite	16.2	–	–
B-g-C_3N_4	35.3	–	–
E-g-C_3N_4	88.0	–	–
Ru-K/graphite	3.8	1.76	4.30
Ru-K/B-g-C_3N_4	24.5	1.80	4.09
Ru-K/E-g-C_3N_4	52.5	1.67	3.76

[a] Obtained by the N_2 adsorption-desorption method through the Brunauer-Emmett-Teller equation.
[b] Analyzed by ICP-AES method.

88.0 $m^2\,g^{-1}$. The light absorption edge of E-g-C_3N_4 locates at a shorter wavelength (Fig. 1b and Fig. S2). Fig. 2a shows E-g-C_3N_4 has a wider optical bandgap than B-g-C_3N_4. A slightly shifted peak in the photoluminence spectrum was found in E-g-C_3N_4 (Fig. S3). The photocurrent of E-g-C_3N_4 in Fig. 2b is also enhanced due to its good electron-hole separation and transport properties. The TEM image of E-g-C_3N_4 is much more transparent (Fig. 3a) than those of g-C (Fig. 3b) and B-g-C_3N_4 (Fig. 3c) [33–39].

After the loading of Ru and K, obvious diffraction peaks attributed to metallic Ru were observed over Ru-K/g-C and Ru-K/B-g-C3N4, which are attributed to the unfavourable dispersion of Ru species on the supports with smaller specific surface areas (Figs. 1a, S1 and Table 1). Over Ru-K/E-g-C_3N_4, no diffraction peaks assigned to metallic Ru were detected (Fig. 1a), suggesting that the Ru nanoparticles were very fine and well dispersed over E-g-C_3N_4. Even though the loadings of K were high (up to ca. 4 wt. %, Table 1), no diffraction peaks attributable to K species were observed in any of the catalysts, indicating that K species were of very small structures, highly dispersed over the three supports (Fig. 1a). The shift of representative diffraction peak for g-C_3N_4 to high values is probably due to the lattice distortion resulted by the doped Ru and K. The dispersion behaviours of Ru particles and K species over the Ru-K catalysts were further confirmed via their TEM images in Fig. 3d–h. As in this study, two metals were loaded onto a specific support, it is important to distinguish the two metals from each other. Here, the crystalline structure and the fast fourier transform (FFT) diffraction spot analysis of all the observable nanoparticles were carried out to identify their compositions, with the nanoparticles displaying in the square of the TEM image of Ru-K/B-g-C_3N_4 in Fig. 3f as a typical example. Its high resolution TEM image (Fig. 3g), together with the FFT diffraction spots at 2.05 Å and 1.35 Å (Fig. 3h) which could be assigned to the (101) and (110) planes of hexagonal close-packed Ru suggest that the nanoparticle was metallic Ru. All the observable nanoparticles were confirmed to be metallic Ru while K species were not detected, indicating K was well dispersed with very small sizes. The average sizes of Ru nanoparticles over Ru-K/E-g-C_3N_4, Ru-K/g-C and Ru-K/B-g-C_3N_4 could be obtained from the TEM images in Fig. 3d–f, and they were 2.8 nm, 6.9 nm and 4.2 nm, respectively. The light absorption properties (Fig. 1b), photoluminence properties (Fig. 2(c)) and the trend in photocurrents (Fig. 2(d)) were not influenced greatly after the loading of Ru and K. The trend in photocurrents is Ru-K/E-g-C_3N_4 > Ru-K/B-g-C_3N_4 > Ru-K/g-C.

The detailed results for photocatalytic ammonia synthesis are displayed in Fig. 4. As expected, g-C exhibited nearly no catalytic activity because of its poor light absorption capacity (Fig. 1b), while B-g-C_3N_4 and E-g-C_3N_4 exhibited some but low activities for ammonia production (0.00–0.08 mmol g^{-1} ammonia production at 10 h reaction), with the activities over the supports conforming to the trend of E-g-C_3N_4 > B-g-C_3N_4 > g-C (Fig. 4a). The higher activity over E-g-C_3N_4 relative to that over B-g-C_3N_4 is due to its larger specific surface area, and more efficient electron/hole separation and transport processes (Table 1 and Fig. 2b) [33–39].

Introducing Ru and K in order to promote N_2 activation increased ammonia production from 0.00-0.08 mmol g^{-1} up to 0.21–0.85 mmol g^{-1} after 10 h reaction (Fig. 4a). We had expected E-g-C_3N_4, combined with the highly dispersed and fine Ru particles on Ru-K/E-g-C_3N_4, to be more active in ammonia synthesis compared to the Ru particles poorly dispersed on B-g-C_3N_4 with lower surface area (Ru-K/B-g-C_3N_4), however, the yield of ammonia production over Ru-K/B-g-C_3N_4 (0.85 mmol g^{-1}) was nearly 2.6 times higher than that over Ru-K/E-g-C_3N_4 (0.33 mmol g^{-1}) after 10 h reaction, opposite to the above expectation. The activity tests, as the function of time in Fig. 4b, further confirmed the trend of ammonia production rates as Ru-K/B-g-C_3N_4 > Ru-K/E-g-C_3N_4 > Ru-K/g-C. ICP-AES analysis of the post-reaction aqueous solutions revealed that the leaching of Ru and K over the catalysts could be neglected during 10 h evaluation (Table S2).

It is considered whether the NH_2/NH groups on g-C_3N_4 would be consumed during the reaction and contribute to ammonia synthesis. It can be stated that the NH_2/NH groups on g-C_3N_4 has negligible contribution to the overall ammonia production due to the following three reasons. (1) Over each of the catalysts, the amount of ammonia

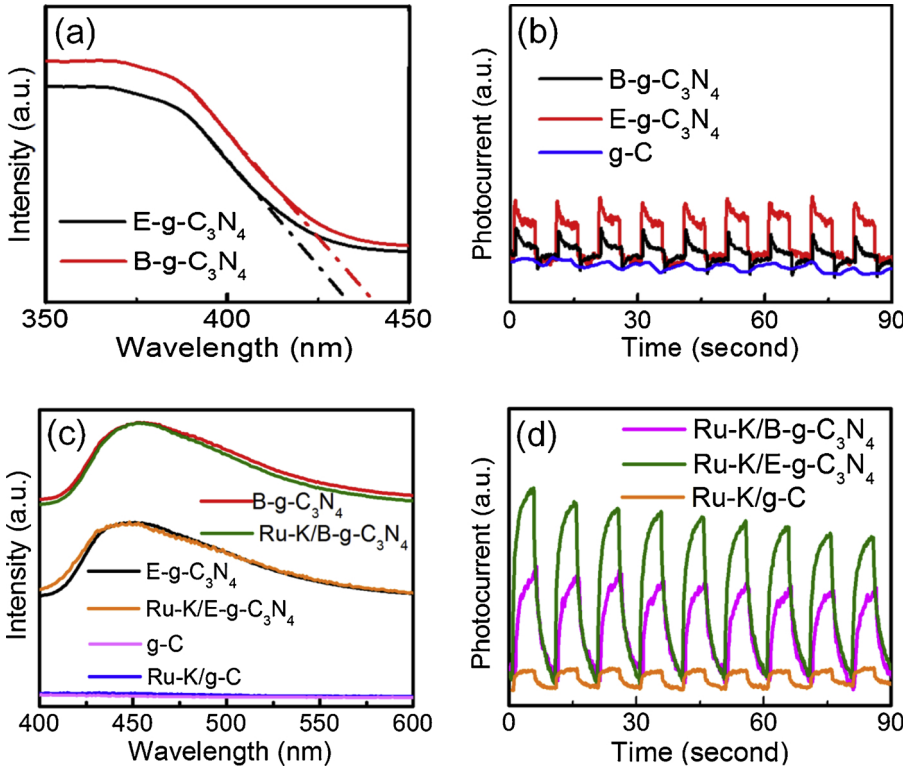

Fig. 2. (a) Enlarged UV–vis spectra of B-g-C_3N_4 and E-g-C_3N_4 in the range of 350–450 nm. (b) Photocurrents over the supports. (c) Photoluminescence spectra and (d) photocurrents of supports and catalysts.

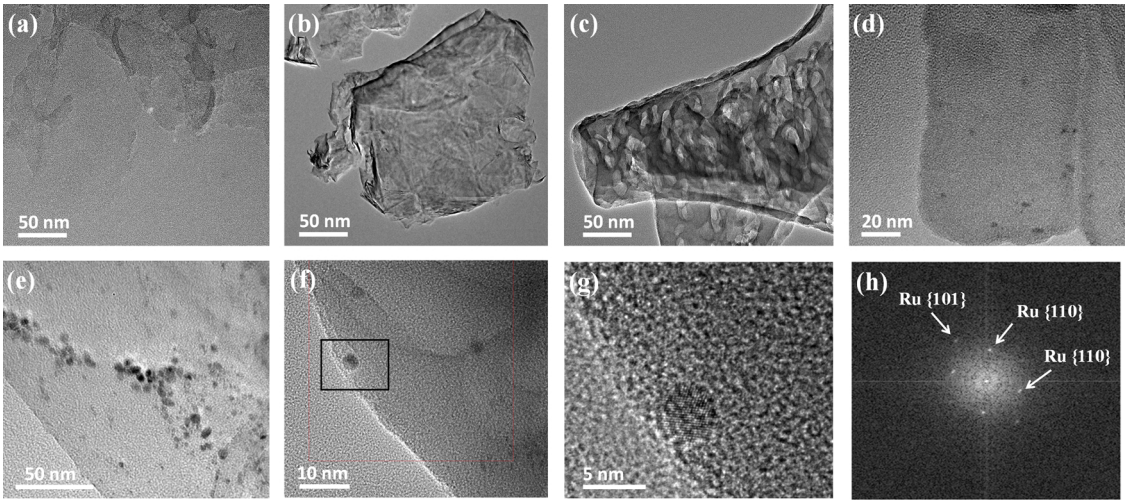

Fig. 3. TEM images of the supports and catalysts. (a) E-g-C_3N_4, (b) g-C, (c) B-g-C_3N_4, (d) Ru-K/E-g-C_3N_4, (e) Ru-K/g-C, (f) Ru-K/B-g-C_3N_4, (g) high resolution TEM image of Ru-K/B-g-C_3N_4 in Fig. 2f, and (h) FFT image of the particle in Fig. 2g.

production increased nearly linearly with reaction time (Fig. 4b), indicating that the ammonia synthesis was not based on the consumption of NH_2/NH groups. The reason is that, if the NH_2/NH group contributed significantly to ammonia production, more ammonia would be generated at the initial stage of the reaction, and the reaction rate decreased gradually with the consumption of NH/NH_2 groups. (2) The sp^3 C—N bond is quite stable and the dissociation energy is about 3.39 eV [52], while the adsorption energy of NH/NH_2 on Ru surface is 1.02/1.72 eV [53]. Thus, the cleavage of C—N bond and formation of Ru-N bond should need high energy to overcome the energy barrier. (3) Given the same molecular formula between E-g-C_3N_4 and B-g-C_3N_4, E-g-C_3N_4 should possess the same amounts of NH_2/NH as B-g-C_3N_4 if the same amounts of g-C_3N_4 were used as photocatalyst, which then leads to comparable or higher photocatalytic performance over E-g-C_3N_4 than B-g-C_3N_4 (by taking the facilitated electron-hole separation over E-g-C_3N_4 into consideration). However, the ammonia yield on B-g-C_3N_4 was higher than E-g-C_3N_4.

Considering that photocatalytic ammonia production is a tandem reaction, comprising two consecutive reactions, photocatalytic H_2 evolution and ammonia synthesis from N_2 and H_2, respectively, photocatalytic H_2 evolution activities over Ru-K/E-g-C_3N_4 and Ru-K/B-g-C_3N_4 were evaluated for reference. It was found that, over a 10 h reaction period, H_2 production amounted to 2.1 mmol g^{-1} and 2.9 mmol g^{-1} over Ru-K/B-g-C_3N_4 and Ru-K/E-g-C_3N_4, respectively. Furthermore, H_2 generation could also be detected over Ru-K/B-g-C_3N_4 and Ru-K/E-g-C_3N_4 catalysts during the ammonia synthesis process.

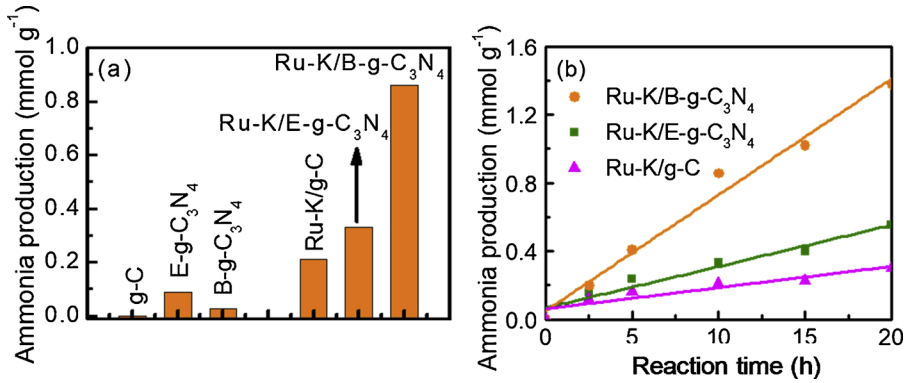

Fig. 4. (a) The amount of ammonia production over the supports and catalysts with a reaction time of 10 h, and (b) effects of reaction time on the amount of ammonia production over Ru-K/B-g-C_3N_4, Ru-K/E-g-C_3N_4 and Ru-K/g-C.

This suggests that H_2 or H radical generation is not the rate-determining step in the ammonia synthesis and that Ru-K/E-g-C_3N_4 exhibits greater activity than Ru-K/B-g-C_3N_4 in photocatalytic reactions, consistent with the greater electron-hole separation capacity of E-g-C_3N_4 [33–39]. We therefore conclude that the second reaction, ammonia synthesis from N_2 and H_2, is the rate-determining step, and that the synergetic effects between Ru and g-C_3N_4 other than photo-properties, must be responsible for the significant enhancement of the N_2 dissociation and reaction with H_2 that lead to the greater ammonia production rate over Ru-K/B-g-C_3N_4.

The TEM image of Ru-K/B-g-C_3N_4 revealed that the Ru particles preferred to stay on the edges of the support B-g-C_3N_4 (Fig. 3f), and a similar phenomenon was also observed for the Ru particles on Ru-K/g-C (Fig. 3e). In contrast, the TEM image of Ru-K/E-g-C_3N_4 in Fig. 3d revealed that the Ru particles were relatively uniformly dispersed on E-g-C_3N_4, and no obvious location preference was observed. As the TEM images (Fig. 3a–c) revealed, E-g-C_3N_4 was monolayer/few-layer structured, while B-g-C_3N_4 and g-C were multilayered. This raised the questions of whether the layered structure of the supports could exert an influence on the locations of Ru particles and K species, which we investigate below.

As described in the catalyst preparation section, Ru and K are loaded onto the catalyst by exposure to aqueous solutions of their salts. We note that the precursors in solution exist as $Ru(H_2O)_6^{3+}$ [54] and K^+, which have cation diameters of 0.42 nm and 0.14 nm [55], respectively. Compared to the layer spacing of ca. 0.32 nm [33–39] in B-g-C_3N_4 and g-C, it is apparent that the observed high degree of dispersion of K is consistent with its being able to move easily into the interlayer region which is not accessible to the larger Ru precursor in these substrates. Instead, over B-g-C_3N_4 and g-C, Ru is concentrated at the step edges between layers presumably because these low-coordinated, high specific surface-energy sites promote Ru nucleation. The more uniform dispersion of Ru over the exfoliated E-g-C_3N_4 in consistent with the limited interlayer space and scant numbers of steps on E-g-C_3N_4. The H_2-TPR profiles of Ru-K/E-g-C_3N_4 in Fig. S4 showed no peak for Ru reduction probably because the Ru NPs is too small and the reduction process was proceeded gradually; while an obvious peak for Ru reduction at around 240–250 ℃ was found in the Ru-K/B-g-C_3N_4, which suggested the interaction between Ru and carbon support is stronger on the Ru-K/B-g-C_3N_4 than the Ru-K/E-g-C_3N_4 due to the edge effect.

We conclude that the unexpected significant enhancement of ammonia production over Ru-K/B-g-C_3N_4 is due to the location of the Ru at the edge steps where apparently poor dispersion nevertheless gives greater activity than the well-dispersed Ru in Ru-K/E-g-C_3N_4. Therefore, DFT calculations were carried out to confirm and explore the underlying reaction mechanisms. To model the Ru-K/E-g-C_3N_4 catalyst, a Ru_{11} cluster was adsorbed on an E-g-C_3N_4 layer where various adsorption sites were considered, and for the Ru-K/B-g-C_3N_4 catalyst, the Ru_{11} cluster was placed at the edge of two layers of g-C_3N_4 (the illustrations of the supports are displayed in Fig. S5). Here, the Ru_{11} cluster was chosen because it is the smallest cluster containing sites like the B_5 step sites, which are viewed as the active centers for N_2 dissociation (the atomic structure of Ru_{11} and the B5 step sites are shown in Figs. S6 and S7). The presence of K was not considered in the simulations for the following three reasons, (1) K was well dispersed over the catalysts, (2) its function as an electron donor for Ru species has been well studied previously [55–57], (3) roughly, the ratio of Ru species to its adjacent K species over Ru-K/E-g-C_3N_4 was 0.5 (Table 1 and Fig. 2), which was a more favourable ratio for ammonia synthesis than that for Ru-K/B-g-C_3N_4 (much larger than 0.5, Table 1 and Fig. 2) according to previous studies [56–58], and (4) the introduced K atom does significantly affect the dissociation energy of N_2 (detailed simulation procedures are

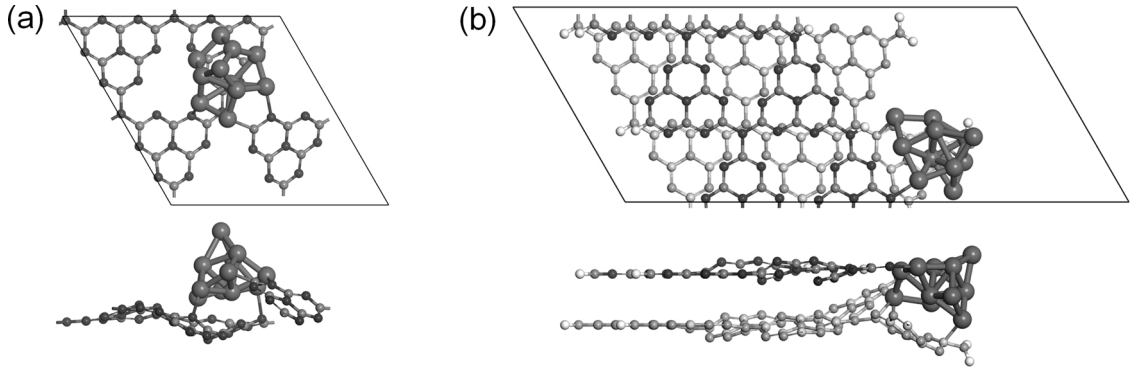

Fig. 5. Top and side views of the most stable geometric structures of Ru_{11} cluster adsorption on (a) E-g-C_3N_4 and (b) B-g-C_3N_4 supports. The small gray and black balls represent C and N atoms. The big gray balls represent Ru atoms. In the second layer of B-g-C3N4, the light gray, light black and white balls represent C, N and H atoms, respectively. (For interpretation of the references to colour in this figure legend, the reader is referred to the web version of this article).

available in supporting information, Figs. S8–S11).

As shown in Fig. 5, it is found that for Ru_{11} on E-g-C_3N_4, the Ru_{11} cluster preferred to adsorb on the junction site where three tri-s-triazine units are linked, with an adsorption energy of −10.21 eV; while on B-g-C_3N_4, the most stable site for the Ru_{11} cluster was on the top of the tri-s-triazine unit, where the adsorption energy was calculated to be −13.77 eV. After the introduction of the Ru_{11} cluster, the distortion of g-C_3N_4 in the Ru/B-g-C_3N_4 catalyst was found to be greater than that in the Ru/E-g-C_3N_4 catalyst, which suggested the sp^2-hybridization of nitrogen and carbon atoms near the edge of B-g-C_3N_4 was changed into sp^3-hybridization, resulting in a much stronger binding between the Ru_{11} cluster and the B-g-C_3N_4 support. The stronger binding between the Ru_{11} cluster and B-g-C_3N_4 support is due to the electronic effects of edge sites [59–62], since Ru_{11} preferentially binds at the edges of B-g-C_3N_4.

In the photocatalytic ammonia synthesis reaction, the Ru_{11} cluster can not only enhance the generation of charge carriers upon light adsorption but also provides an active centre for the proton reduction and ammonia synthesis. The ability of the Ru cluster to trap electrons is determined by the work function of the Ru [63,64]. In our systems, considering the work function of bulk Ru of 5.4 eV [65], the work function of Ru_{11} cluster should be larger than those of E-g-C_3N_4 (4.13 eV) and two-layered g-C_3N_4 (3.93 eV) [66] (Figs. S13–S14), which indicates electrons flow from E-g-C_3N_4 and B-g-C_3N_4 into the Ru clusters on contact. The negatively charged Ru_{11} cluster on the g-C_3N_4 support not only can greatly promote the photocatalytic activities of E-g-C_3N_4 and B-g-C_3N_4, in agreement with our experimental results (Fig. 1b), but also mimic the function of the MoFe-cofactor in nitrogenase for N_2 reduction to NH_3 [67,68]. In the following we consider two reaction paths of ammonia synthesis, including the direct N_2 dissociation and associative N_2 dissociation mechanisms [69]. As shown in Fig. 6a, for the system of Ru/E-g-C_3N_4, initially N_2 favoured adsorption on the Ru atom of the Ru_{11} cluster perpendicularly, with an adsorption energy of -2.18 eV. Along the favourable reaction path, N_2 assumed a more parallel orientation to the surface with both N atoms bonding to the Ru_{11} cluster. This "lying-down" configuration was less stable (by 0.83 eV than the perpendicular geometry). The energy barrier from the "perpendicular" to "lying-down" orientation was calculated to be 1.13 eV. Subsequently, N_2 may undertake two different activation pathways: (1) direct N_2 dissociation, in which N_2 directly dissociates into two N atoms with the energy barrier of 1.00 eV; or alternatively (2) associative N_2 dissociation, in which the "lying-down" N_2 molecule was firstly hydrogenated to form $*N_2H$ and then dissociated into *N and *NH, with energy barriers of 0.81 eV and 0.41 eV respectively. Therefore, over Ru/E-g-C_3N_4, the rate-limiting step is the change in N_2 orientated from the "perpendicular" to "lying-down" state, with the energy barrier for N_2 activation of 1.13 eV, and the associative reaction mechanism significantly more favourable than the direct N_2 dissociation mechanism.

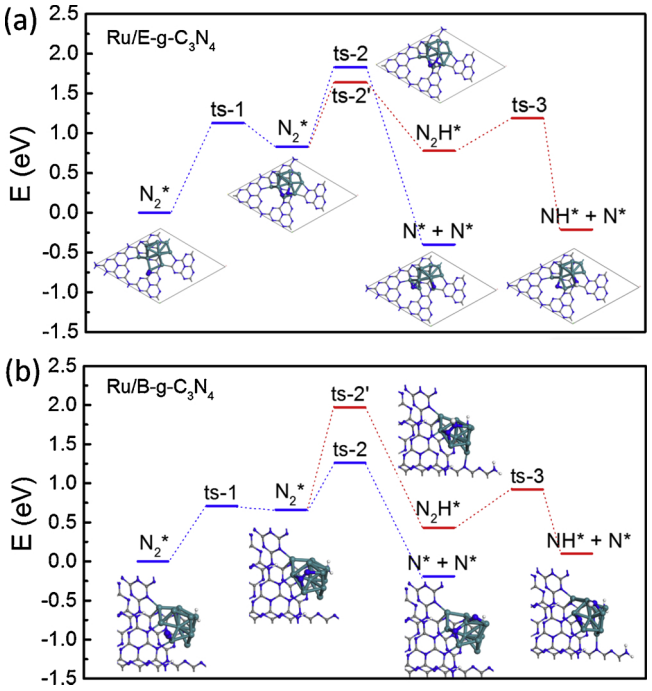

Fig. 6. Direct N_2 dissociation and associative N_2 dissociation reaction mechanisms over (a) Ru/E-g-C_3N_4 and (b) Ru/B-g-C_3N_4. The reference energy (the total energy of the initial N_2 adsorption state over both supports) is set zero.

Fig. 6b illustrates the two N_2 dissociation paths (direct and associative) over Ru/B-g-C_3N_4. Similarly, N_2 initially adsorbed on the Ru_{11} cluster in a perpendicular orientation with an adsorption energy of −1.31 eV, which was lower than that on the Ru/E-g-C_3N_4 catalyst. Then, N_2 tilted and changed to a "lying-down" configuration, with an energy barrier of 0.71 eV. Following, (1) the "lying-down" N_2 can be directly dissociated with an energy barrier of just 0.60 eV, much lower than that over Ru/E-g-C_3N_4; or (2), for the associative dissociation path, the energy barriers of N_2 hydrogenation to $*N_2H$ and dissociation of $*N_2H$ into *N and *NH were 1.31 eV and 0.49 eV, respectively. Therefore, the direct N_2 dissociation path was much more favourable over the Ru/B-g-C_3N_4 catalyst. The tilting process of N_2 over Ru/B-g-C_3N_4 is the rate-limiting step, and the energy barrier was 0.71 eV.

The DFT results revealed that the two catalysts exhibited different underlying mechanisms for N_2 activation, namely an associative dissociation path over Ru/E-g-C_3N_4, and a direct dissociation path over Ru/B-g-C_3N_4. They, however, exhibited the same rate determining step, that is, the transition of N_2 from a perpendicular geometry to "lying down" geometry, where the energy barrier of the transition state over Ru/E-g-C_3N_4 (1.13 eV) was 0.42 eV higher than that over Ru/B-g-C_3N_4 (0.71 eV). The energy barriers 1.13 eV and 0.71 eV could be easily satisfied by light irradiation, which is why ammonia could be produced over the catalysts with light irradiation. The relative low energy barrier of the rate-limiting step over Ru/B-g-C_3N_4 suggested that the reaction rate of ammonia production over Ru/B-g-C_3N_4 will be superior to Ru/E-g-C_3N_4, in accordance with our experimental results of catalytic activity for ammonia synthesis. The lower energy barrier over Ru/B-g-C_3N_4 is attributed to the stronger binding between the Ru_{11} cluster and the support, which reduces the interaction between N_2 and Ru_{11} cluster.

4. Conclusions

In summary, the physicochemical properties of the catalysts and the evaluation results revealed that, in contrast to our general understanding that the catalyst with faster electron/hole separation rate and higher photocurrent as well as fine and well dispersed metal nanoparticles (Ru-K/E-g-C_3N_4) should exhibit better photocatalytic activity, Ru-K/B-g-C_3N_4 yielded higher photocatalytic ammonia production rate than Ru-K/E-g-C_3N_4. It is suggested that the light harvesting properties of the catalysts must cooperate with the surface reaction properties to facilitate the ammonia synthesis process. Ru nanoparticles at the edge steps over the multilayered bulk support (B-g-C_3N_4) contributed higher surface reactivity than the Ru nanoparticles uniformly and randomly dispersed over monolayered E-g-C_3N_4 in N_2 reduction with H_2. Our theoretical studies revealed that the Ru nanoparticles located at the edges possessed stronger binding with the support and exhibited a lower reaction barrier for N_2 activation, which is ultimately responsible for the much-enhanced photocatalytic ammonia synthesis rate over Ru-K/B-g-C_3N_4. In this study, the relationship between photocatalytic reactivity and support geometry was discovered, which will be important in guiding the rational predesign of efficient photocatalysts.

Author contributions

All authors have given approval to the final version of the manuscript.

Acknowledgment

J.H. and C.S. acknowledge the financial supports from Australian Research Council Discovery Projects (DP150103842). J.H., C.S., and X.L. acknowledge the financial supports from Sydney Nano Grand Challenge Project. We also acknowledge computational resources provided by the Australian National Computational Infrastructure (NCI).

Appendix A. Supplementary data

Supplementary material related to this article can be found, in the online version, at doi:https://doi.org/10.1016/j.apcatb.2019.118026.

References

[1] M. Kitano, Y. Inoue, Y. Yamazaki, F. Hayashi, S. Kanbara, S. Matsuishi, T. Yokoyama, S. Kim, M. Hara, H. Hosono, Nat. Chem. 4 (2012) 934–940.
[2] S. Licht, B. Cui, B. Wang, F. Li, J. Lau, S. Liu, Science 345 (2014) 637–640.
[3] K. Honkala, A. Hellman, I.N. Remediakis, A. Logadottir, A. Carlsson, S. Dahl, C.H.J.K. Christensen, Science 307 (2005) 555–558.
[4] J.W. Erisman, M.A. Sutton, J. Galloway, Z. Klimont, W. Winiwarter, Nat. Geosci. 1 (2008) 636–639.
[5] T. Kandemir, M.E. Schuster, A. Senyshyn, M. Behrens, R. Schlçgl, Angew. Chem. Int. Ed. 52 (2013) 12723–12726.
[6] D.K. Spaulding, G. Weck, P. Loubeyre, F. Datchi, P. Dumas, M. Hanfland, Nat. Commun. 5 (2014) 5739.
[7] J. Li, H. Li, G. Zhan, L. Zhang, Acc. Chem. Res. 50 (2017) 112–121.
[8] B. Askevold, J.T. Nieto, S. Tussupbayev, M. Diefenbach, E. Herdtweck, M.C. Holthausen, S. Schneider, Nat. Chem. 3 (2011) 532–537.
[9] G.N. Schrauzer, T.D. Guth, J. Am. Chem. Soc. 99 (1977) 7189–7193.
[10] Q. Wu, R.J. Am, Chem. Soc. 134 (2012) 9369–9375.
[11] S. Wang, X. Hai, X. Ding, K. Chang, Y. Xiang, X. Meng, Z. Yang, H. Chen, J. Ye, Adv. Mater. 29 (2017) 1701774.
[12] S. Kozuch, S. Shaik, S. Shaik, S. Shaik, Acc. Chem. Res. 44 (2011) 101–110.
[13] M. Kitano, S. Kanbara, Y. Inoue, N. Kuganathan, P.V. Sushko, T. Yokoyama, M. Hara, H. Hosono, Nat. Commun. 6 (2015) 6731.
[14] J.J. Mortensen, L.B. Hansen, B.J.K. Hammer, J. Catal. 182 (1999) 479–488.
[15] R. Jonathan, P.J. Jonas, Am. Chem. Soc. 138 (2016) 4243–4248.
[16] Á.J.K.J. Logadóttir, Catal. J. Catal. 220 (2003).
[17] S.E. Siporin, R.J. Davis, J. Catal. 225 (2004) 359–368.
[18] L. He, L. Jing, Y. Luan, L. Wang, H. Fu, ACS Catal. 4 (2014) 990–998.
[19] N.N. Rao, S. Dube, M.P. Natarajan, Appl. Catal. B: Environ. 5 (1994) 33–42.
[20] D.L. Boucher, J.A. Davies, J.G. Edwards, A.J. Mennad, Photoch. Photobio. A: Chem. 88 (1995) 53–64.
[21] N.D. Dien, L.H. Phuoc, V.X. Hien, D.D. Vuong, N.D. Chien, J. Korean Inst. Electr. Electron. Mater. Eng. 46 (2017) 3309–3316.
[22] X. Pan, X. Bao, Accounts Chem. Res. 44 (2011) 553–562.
[23] W. Chen, Z. Fan, X. Pan, X. Bao, X. Pan, X.J. Bao, Am. Chem. Soc. 130 (2008) 9414–9419.
[24] G. Chen, C. Xu, X. Huang, J. Ye, L. Gu, G. Li, Z. Tang, B. Wu, H. Yang, Z. Zhao, Z. Zhou, G. Fu, N. Zheng, Nat. Mater. 15 (2016) 564–569.
[25] J. Kibsgaard, Z. Chen, B.N. Reinecke, T.F. Jaramillo, Nat. Mater. 11 (2012) 963–969.
[26] Z. Wang, B. Liu, J. Lin, Appl. Catal. A Gen. 458 (2013) 130–136.
[27] L. Li, Y. Wang, S. Vanka, X. Mu, Z. Mi, C. Li, Angew. Chem. Int. Ed. 56 (2017) 8701–8705.
[28] Z. Ma, X. Xiong, C. Song, B. Hu, Zhang, W. RSC Adv. 6 (2016) 51106–51110.
[29] K. Nakatsuka, Y. Kuwahara, K. Mori, H. Yamashita, Chem. Lett. 44 (2015) 1691–1693.
[30] A. Takagaki, M. Sugisawa, D. Lu, J.N. Kondo, M. Hara, K. Domen, S. Hayashi, J. Am. Chem. Soc. 125 (2003) 5479–5485.
[31] X. Yu, M.S. Prevot, N. Guijarro, K. Sivula, Nat. Commun. 6 (2015) 8596.
[32] X. Hai, K. Chang, H. Pang, M. Li, P. Li, H. Liu, L. Shi, J. Ye, J. Am. Chem. Soc. 138 (2016) 14962–14969.
[33] X. Wang, K. Maeda, A. Thomas, K. Takanabe, G. Xin, J.M. Carlsson, K. Domen, M. Antonietti, Nat. Mater. 8 (2009) 76–80.
[34] S. Yang, Y. Gong, J. Zhang, L. Zhan, L. Ma, Z. Fang, R. Vajtai, X. Wang, P.M. Ajayan, Adv. Mater. 25 (2013) 2452–2456.
[35] Y. Hou, A.B. Laursen, J. Zhang, G. Zhang, Y. Zhu, X. Wang, S. Dahl, I. Chorkendorff, Angew. Chem. Int. Ed. 52 (2013) 3621–3625.
[36] G. Dong, W. Hob, C.J. Wang, J. Mater. Chem. A Mater. Energy Sustain. 3 (2015) 23435–23441.
[37] P. Niu, G. Liu, G. Cheng, J. Phys. Chem. C 116 (2012) 11013–11018.
[38] C. Xu, K. Li, W.J. Zhang, Colloids Interface Sci. Commun. 495 (2017) 27–36.
[39] Y. Shiraishi, S. Shiota, Y. Kofuji, M. Hashimoto, K. Chishiro, H. Hirakawa, S. Tanaka, S. Ichikawa, Takayuki Hirai, ACS Appl. Energy Mater. 1 (2018) 4169–4177.
[40] A. Thomas, A. Fischer, F. Goettmann, M. Antonietti, J. Müller, R. Schlögl, J. Carlsson, M. J. Mater. Chem. 18 (2008) 4893–4908.
[41] X. Zhang, X. Xie, H. Wang, J. Zhang, B. Pan, Y.J. Xie, Am. Chem. Soc. 135 (2013) 18–21.
[42] G. Kresse, J.J. Furthmüller, Comput. Mat. Sci. 6 (1996) 15–50.
[43] G. Kresse, Furthmüller, J. Phys. Rev. B 54 (1996) 11169–11186.
[44] J.P. Perdew, K. Burke, M. Ernzerhof, Phys. Rev. Lett. 77 (1996) 3865–3868.
[45] S. Grimme, J. Antony, S. Ehrlich, S.J. Krieg, Chem. Phys. 132 (2010) 154104.
[46] G.U. Henkelman, B.P. Uberuaga, H. Jonsson, J. Chem. Phys. 113 (2000) 9901.
[47] S. Zuluaga, L.H. Liu, N. Shafiq, S.M. Rupich, J.F. Veyan, Y.J. Chabal, T. Thonhauser, Phys. Chem. Chem. Phys. 17 (2015) 957–962.
[48] X. Ma, Y. Lv, J. Xu, Y. Liu, R. Zhang, Y. Zhu, J. Phys. Chem. C 116 (2012) 23485–23493.
[49] A.E. Torres, T. Pandiyan, F. Colmenares, J. Mex. Chem. Soc. 56 (2012) 287–293.
[50] S. Park, J. An, J.R. Potts, A. Velamakanni, S. Murali, R.S. Ruoff, Carbon 49 (2011) 3019–3023.
[52] A.L. Norbert, G.S. James, Lange's Handbook of Chemistry, McGraw-Hill, New York, 2005 1.
[53] A.J. Medford, J. Wellendorff, A. Vojvodic, F. Studt, F. Abild-Pedersen, K.W. Jacobsen, T.J.K. Bligaard, Science 345 (2014) 197–200.
[54] J. Lee, D. Pyo, Y. Lee, X. Yang, S. Ryu, Indian J. Eng. Mater. Sci. 17 (2010) 327–330.
[55] D. Kurzydłowski, M. Derzsi, A. Budzianowski, Z. Jaglicic, W. Kozminski, Z. Mazej, W. Grochala, Eur. J. Inorg. Chem. 19 (2010) 2919–2925.
[56] W. Jiang, Y. Li, W. Han, Y. Zhou, H. Tang, H.J. Liu, Energy Fuels 23 (2014) 443–452.
[57] K. Aika, Catal. Today 286 (2017) 14–20.
[58] N. Saadatjou, A. Jafari, S. Sahebdelfar, Chem. Eng. Commun. 202 (2015) 420–448.
[59] X.A. Peng, Q. Wei, J. Appl. Phys. 116 (2014) 144301.
[60] K. Nakada, M. Fujita, Phys. Rev. B 54 (1996) 17954–17961.
[61] Q. Tang, Y. Cui, Y. Li, Z. Zhou, Z. Chen, J. Phys. Chem. C 115 (2011) 1724–1731.
[62] S. Bhattacharyya, Y. Kawazoe, A.K. Singhl, J. Nanosci. Nanotechnol. 12 (2012) 1899–1902.
[63] Y. Di, X. Wang, A. Thomas, M. Antonietti, ChemCatChem 2 (2010) 834–838.
[64] D.E. Jiang, M.H. Du, S. Dai, J. Chem. Phys. 130 (2009) 074705.
[65] D.W. Wood, Phys. Rev. Lett. 46 (1981) 749.
[66] D.R. Dean, J.T. Bolin, L.J. Zheng, Bacteriol 175 (1993) 6737–6744.
[67] H. Li, C. Mao, H. Shang, Z. Yang, Z. Ai, L. Zhang, Nanoscale 10 (2018) 15429.
[68] A.L. Garden, E. Skúlason, J. Phys. Chem. C 119 (2015) 26554–26559.

Further reading

[51] A. Kalytta-Mewes, S. Spirkl, S.Tränkle, M.Hambach, D. Volkmer. J. Mater. Chem. A Mater. Energy Sustain. 2015; 3: 20919-20926